Research Square

Preprints are preliminary reports that have not undergone peer review.
They should not be considered conclusive, used to inform clinical practice,
or referenced by the media as validated information.

Cardioprotective effects of Cinnamomum migao water extract against acute myocardial infarction: insights from integrated untargeted and spatial metabolomics into glycerophospholipid metabolism and SRC/PI3K/AKT signaling

Zuying Zhou
Guizhou Medical University
Yue Peng
Guizhou Medical University
Ling cao
Guizhou Medical University
Chunxian Zhu
Guizhou Medical University
Siying Chen
Guizhou Medical University
Zipeng Gong
Guizhou Medical University
Yueting Li
Guizhou Medical University
Mingyan Chi
Guizhou Medical University
Yong Huang
huangy2020@126.com
Guizhou Medical University
Wenxiang Fan
Guizhou Medical University
Lin Zheng
Guizhou Medical University

Research Article

Keywords: Cinnamomum migao, Acute myocardial infarction, Glycerophospholipid metabolism, Spatial metabolomics, SRC/PI3K/AKT signaling

Posted Date: November 9th, 2026

DOI: https://doi.org/10.21203/rs.3.rs-11190916/v1

License: This work is licensed under a Creative Commons Attribution 4.0 International License.
Read Full License

Additional Declarations: No competing interests reported.

Cardioprotective effects of *Cinnamomum migao* water extract against acute myocardial infarction: insights from integrated untargeted and spatial metabolomics into glycerophospholipid metabolism and SRC/PI3K/AKT signaling

Zuying Zhou[1,#], Yue Peng[1,#], Ling Cao[1], Chunxian Zhu[1], Siying Chen[1,2], Zipeng Gong[1], Yueting Li[1,2], Mingyan Chi[1], Yong Huang[1,2*], Wenxiang Fan[1,*], Lin Zheng[1,2,*]

1 State Key Laboratory of Discovery and Utilization of Functional Components in Traditional Chinese Medicine, School of Pharmaceutical Sciences, Guizhou Key Laboratory of Modern Traditional Chinese Medicine Creation, Guizhou Medical University, Anshun 561113, China;

2 National Engineering Research Center of Miao's Medicines, Engineering Research Center for the Development and Application of Ethnic Medicine and TCM (Ministry of Education), Guizhou Medical University, Anshun 561113, China;

[#] These authors contributed equally to this work.

[*] Yong Huang(huangy2020@126.com), Wenxiang Fan (fwx13990706098@163.com), and Lin Zheng (ZHENGL2020@126.com).

Abstract

Background

Acute myocardial infarction (AMI) induces profound metabolic disturbances that aggravate cardiomyocyte injury and impair cardiac function. Modulating these disturbances may provide novel strategies for myocardial protection. *Cinnamomum migao*, a traditional ethnic medicinal herb for cardiovascular disorders, is historically administered as a decoction. While previous studies have focused on its volatile oil fraction, the cardioprotective effects and mechanisms of its water extract (CMW), consistent with traditional use, remain insufficiently characterized.

Purpose

This study aimed to systematically evaluate the cardioprotective effects of CMW against AMI and elucidate the underlying mechanisms associated with its metabolic regulation.

Methods

A mouse AMI model was established by left anterior descending coronary artery ligation. Cardioprotective effects of CMW were assessed via electrocardiography, infarct size, serum biomarkers, and histopathology. LC-HRMS-based untargeted metabolomics combined with AFADESI mass spectrometry imaging was employed to characterize myocardial metabolic alterations and spatial distribution of key metabolites. Serum pharmacochemistry, target prediction, and molecular validation were further applied to explore potential mechanisms.

Results

CMW markedly attenuated AMI-induced myocardial injury, evidenced by reduced infarct size, decreased serum biomarkers, and improved histopathology. Metabolomics revealed that CMW reversed AMI-associated disturbances, with glycerophospholipid metabolism identified as a key pathway. AFADESI imaging confirmed partial normalization of phosphocholine, lysophosphatidylcholine (22:5), and glycerophosphocholine distribution. Serum pharmacochemistry identified absorbed constituents including chlorogenic acid, neochlorogenic acid, naringin, afzelin, quercitrin, and norboldine. Molecular validation demonstrated that CMW activated SRC/PI3K/AKT signaling and restored Bcl-2/Bax balance in AMI myocardium.

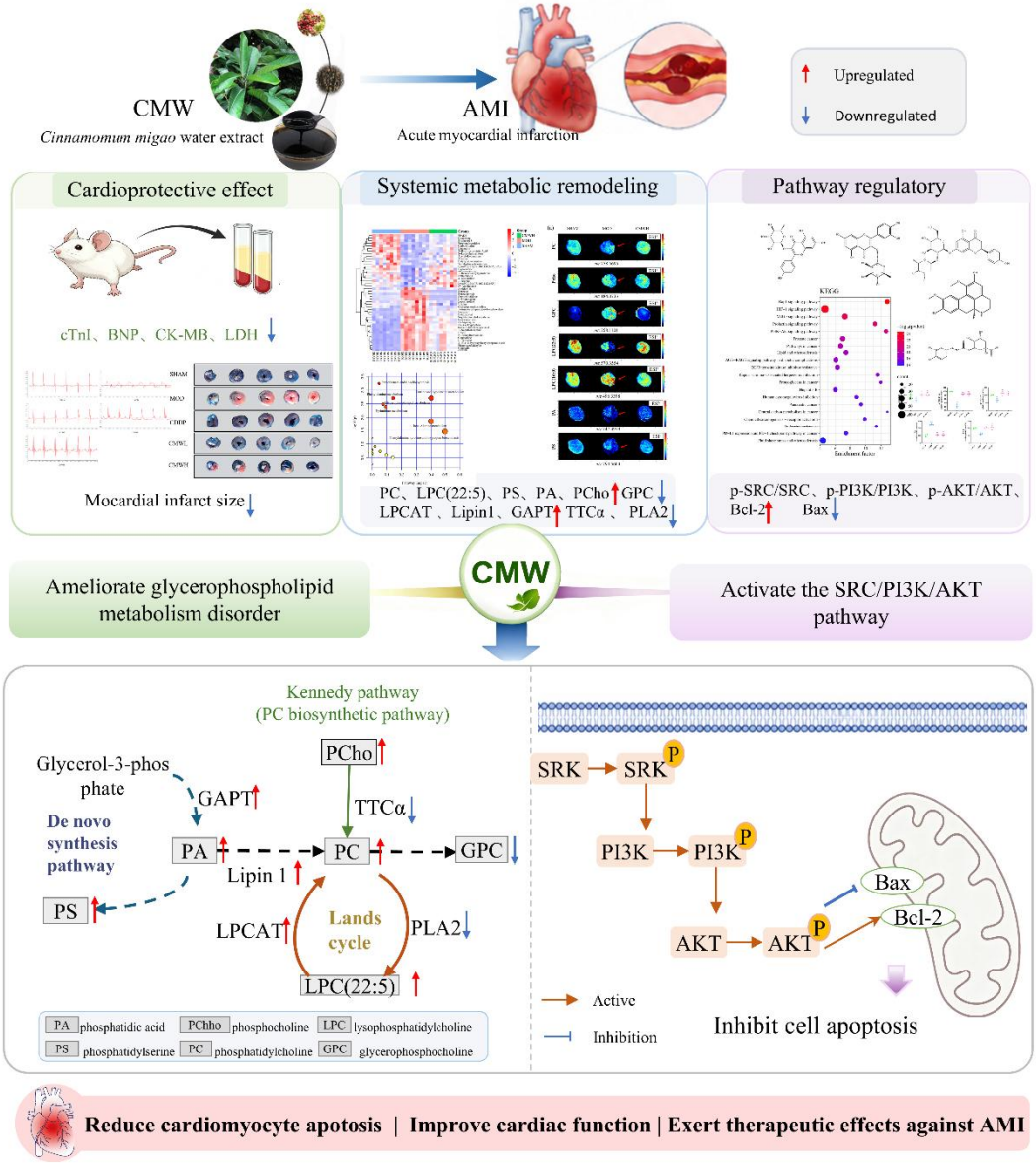
Conclusion

CMW exerts cardioprotective effects against AMI by ameliorating glycerophospholipid metabolic disturbances and activating SRC/PI3K/AKT-associated signaling. Integration of untargeted and spatial metabolomics provides complementary evidence for its metabolic regulatory actions, offering a modern pharmacological interpretation of the traditional decoction use of *Cinnamomum migao*.

Key words

Cinnamomum migao; Acute myocardial infarction; Glycerophospholipid metabolism; Spatial metabolomics; SRC/PI3K/AKT signaling

Graphical Abstract



1 Introduction

Acute myocardial infarction (AMI) is a critical cardiovascular emergency caused by abrupt coronary artery occlusion, resulting in sustained ischemia-hypoxia and extensive cardiomyocyte necrosis[1]. Clinically, AMI manifests as severe chest pain, chest tightness and palpitations, and is associated with high morbidity and mortality, posing a major threat to public health[2]. Current therapeutic strategies, including percutaneous coronary intervention (PCI) and coronary artery bypass grafting (CABG), aim to restore coronary reperfusion, but are often complicated by postoperative adverse events and reperfusion injury[3, 4]. Moreover, long-term pharmacotherapy with

antiplatelet agents, β-blockers, ACE inhibitors or statins, while beneficial, is constrained by several limitations: single-target mechanisms, drug resistance, cumulative adverse reactions, and poor tolerance in elderly or multi-morbid patients. These shortcomings highlight the urgent need for novel, multi-target interventions that can complement existing therapies and reduce complications[5-7].

Traditional Chinese medicine (TCM) and ethnic herbal medicines, characterized by multi-component and multi-target holistic regulation, have demonstrated promising efficacy in cardiovascular diseases[8]. Clinical evidence supports the use of herbal preparations such as Shexiang Baoxin Pills and Compound Danshen Dropping Pills in perioperative intervention, postoperative combined therapy and long-term rehabilitation of AMI patients[9, 10]. Importantly, AMI is essentially a metabolic disorder: persistent ischemia-hypoxia disrupts cardiomyocyte metabolic networks, particularly lipid metabolism, leading to progressive cardiac dysfunction. Glycerophospholipid metabolic imbalance has been identified as a key driver of cardiomyocyte injury, apoptosis and impaired tissue repair[11, 12]. Thus, restoring myocardial metabolic homeostasis has emerged as a novel therapeutic target for acute myocardial injury.

Cinnamomum migao, a distinctive ethnic medicinal resource from southwest China, has long been used to dispel cold-dampness, promote qi, and relieve pain, and is traditionally applied for coronary heart disease, angina pectoris and arrhythmia[13]. Previous pharmacological studies have mainly focused on its volatile oil fraction, which exhibits anti-arrhythmic, anti-ischemic and anti-hypoxia activities[14, 15]. However, folk practice predominantly employs water decoction, suggesting that bioactive constituents exist in aqueous extracts. Preliminary evidence indicates that *Cinnamomum migao* water extract (CMW) reduces myocardial injury biomarkers and alleviates pathological damage, yet systematic studies on its cardioprotective mechanisms remain scarce[16]. This mismatch between traditional decoction usage and volatile-oil-oriented research risks overlooking non-volatile bioactive compounds and hinders rational utilization of limited natural resources.

To address this gap, we hypothesized that CMW confers cardioprotection against AMI by ameliorating glycerophospholipid metabolic disturbances and modulating pivotal signaling pathways. To test this hypothesis, we established a mouse AMI model via left anterior descending coronary artery ligation and adopted a comprehensive multi-omics strategy. Specifically, LC-HRMS

untargeted metabolomics was employed to capture global metabolic reprogramming, while AFADESI mass spectrometry imaging provided tissue-level visualization of metabolite distribution, enabling direct assessment of spatial heterogeneity in myocardial metabolic remodeling. This integration of untargeted and spatial metabolomics represents a methodological innovation, allowing simultaneous characterization of systemic metabolic regulation and localized metabolic alterations within ischemic myocardium.

In parallel, serum pharmacochemistry was applied to identify absorbed constituents of CMW, and network pharmacology combined with molecular validation was used to uncover mechanistic pathways. This multi-layered design not only clarifies the metabolic regulatory effects of CMW but also provides modern pharmacological evidence supporting the traditional decoction use of *Cinnamomum migao*. By integrating metabolomics, spatial metabolomics, pharmacochemistry and molecular biology, this study highlights both the technical and experimental innovations, offering new insights into ethnic medicine-based cardioprotection and advancing the translational potential of CMW in AMI therapy.

2 Materials and methods

2.1 Reagents

The chemicals were listed as follows: Compound Danshen Dripping Pills (CDDP) was provided by TianShili Pharmaceutical Group Co., Ltd.(No.T231206); 2,2,2-tribromoethanol (C2503300) and CMC-Na (I2116097) were purchased from Shanghai Aladdin Reagents Co., Ltd.; 0.9% Sodium Chloride Injection(E124070406) was purchased from Guizhou Kelun Pharmaceutical Co., Ltd.; Brain Natriuretic Peptide (BNP) Assay Kit (ZC-38511), Creatine Kinase Isoenzyme (CK-MB) Assay Kit (ZC-38269) and Troponin-I (cTnI) Assay Kit (ZC-38813) were purchased from Shanghai Zhucai Biotechnology Co., Ltd.; Lactate Dehydrogenase (LDH) Kit (A020-2) was purchased from Nanjing Institute of Biotechnology has been established.; 4% paraformaldehyde (1950136) was purchased from Pinofei Biotechnology Co., Ltd.; Evans blue (C16929983) was purchased from McClin Biochemical Technology Co., Ltd.; 2, 3, 5-TTC (T8170) was purchased from Beijing SuoLarBio Technology Co., Ltd.; Suturelocking needle (240408) was purchased from Ningbo Medical Suture Needle Co., Ltd.; Mass spectrometry-grade methanol (NO213443), formic

acid (NO205178) and Mass spectrometry-grade acetonitrile (NO194035) were purchased from Thermo Fisher Scientific Inc.; Eastep® Super Total RNA Extraction Kit (0000649338) was purchased from ProMerg (Beijing) Biotechnology Co., Ltd.; TB Green® Premix Ex Taq™ II (A071194A) and Prime Scrip™ RT Master Mix (AQ11067A) were purchased from Baorui Medical Biotechnology (Beijing) Co., Ltd.; RIPA lysate (G2002-100ML), 50×Cocktail Protease Inhibitor (G2006-250UL), BCA Protein Quantification Kit (G2026-200T), 10% PAGE Colorful Gel Ultra-Rapid Preparation Kit (G2043-50T), PVDF membrane 0.45 μm (WGPVDF45), Super-High Sensitivity ECL Chemiluminescence Kit (G2020-25ML), TBST buffer solution (G2150-1L), Bovine Serum Albumin (BSA) (GC305010), 20×Tris-EDTA Antigen Retrieval Solution (G1203) and Histochemical Kit–DAB Color Developer (G1212) were purchased from Servicebio.

The antibodies were listed as follows: HRP-conjugated goat anti-rabbit secondary antibody (GB23303; Servicebio); Rabbit Monoclonal Antibody to Vinculin (GB111328; Servicebio); Rabbit Monoclonal Antibody to PI3K (GB11525; Servicebio); Rabbit Monoclonal Antibody to AKT (GB15689;Servicebio); Rabbit Monoclonal Antibody to p-AKT(GB150002;Servicebio); Rabbit Monoclonal Antibody to SRC (GB152343; Servicebio); Rabbit Monoclonal Antibody to Bcl-2 (GB154380; Servicebio); Rabbit Monoclonal Antibody to Bax (GB15690; Servicebio); Rabbit Monoclonal Antibody to p-PI3K (AF3242) and p-SRC (AF3162) were purchased from Jiangsu Qinke Biological Research Center Co., Ltd.

2.2 Preparation of CMW

CMW extract was prepared as follows. *Cinnamomum migao* raw materials (6 kg) were pulverized, immersed in 8-fold purified water for 30 min, and extracted by boiling for 1 h. After filtration, residues were subjected to a second extraction with 8-fold purified water under identical the same conditions. The combined filtrates were concentrated and lyophilized, resulting in a paste yield of 17.68%. The dried extract powder was sealed and stored in a dry environment. For oral gavage administration, the powder was suspended in 0.5% CMC-Na solution and ultrasonicated for 20 min. According to the 2019 Guizhou Provincial Quality Standard for Chinese Medicinal Materials and Ethnic Medicines, the low-dose (CMWL) and high-dose (CMWH) groups were administered at 723.99 and 2171.97 mg/kg, respectively.

2.3 Establishment of the AMI and treatment with CMW/ Compound Danshen Drop Pills[17, 18]

Specific pathogen-free male ICR mice aged 8 weeks were obtained from Changsha Tianqin Biotechnology Co., Ltd. [certificate no. SCXK (Xiang) 2024-0023]. The mice were housed under standard laboratory conditions (18-25 °C, 50%-70% relative humidity) and allowed to acclimatize for one week before experimentation. One hundred mice were randomly assigned into five groups: the SHAM, MOD, CDDP (119.89 mg/kg), CMWL, and CMWH groups. Mice in the SHAM, MOD, CMWL, and CMWH groups received 0.5% CMC-Na as the vehicle control. Mice were anesthetized intraperitoneally with tribromoethanol (20 mL/kg). The AMI model was established by permanent ligation of the left anterior descending (LAD) coronary artery, whereas mice in the SHAM group underwent the same surgical procedure without coronary artery ligation. Corresponding treatments were administered by gavage (10 mL/kg) once daily for 7 consecutive days, beginning 24 h after surgery. 24 h after the last gavage, mice were re-anesthetized with tribromoethanol for electrocardiographic recording and subsequent tissues collection.

2.4 Electrocardiogram examination

Electrocardiographic recordings were obtained using a lead II electrocardiograph. Mice with abnormal baseline electrocardiographic signals were excluded from subsequent analysis. For each group, electrocardiographic signals were continuously recorded for 3-5 min. The successful establishment of the AMI model was initially confirmed by comparing electrocardiographic changes before and after surgery, the presence of ST-segment elevation and abnormal Q waves was used as an indicator of successful AMI induction. At 24 h after the final administration, electrocardiographic parameters were further analyzed to evaluate the protective effects of CMW treatment against AMI.

2.5 Cardiac histopathological examination

Mouse cardiac tissues were fixed in 4% paraformaldehyde for 24 h, followed by routine histological processing, including dehydration, paraffin embedding, sectioning, hematoxylin and eosin (H&E) staining, and mounting. Microscopic images were acquired at low magnification and at 100× and 400× magnifications to assess myocardial structural alterations and inflammatory cell infiltration.

2.6 Measurement of serum cardiac injury biomarkers

Serum samples from each group were collected and analyzed for the levels of lactate dehydrogenase (LDH), creatine kinase-MB (CK-MB), cardiac troponin I (cTnI), and B-type natriuretic peptide (BNP) using commercially available assay kits according to the manufacturers' instructions.

2.7 Evans blue-TTC staining

A 2% Evans blue solution was slowly perfused through the ascending aorta to delineate the non-risk myocardium. Once the myocardium was completely stained blue, hearts were rapidly harvested and rinsed with normal saline. Each mouse heart was sectioned into five uniform transverse slices, which were incubated with 1% triphenyltetrazolium chloride (TTC) solution for 30 min and rinsed with saline. Both sides of the slices were immediately photographed, and infarct areas were quantified using ImageJ software.

2.8 Untargeted metabolomics analysis of cardiac tissues

A 30-mg sample of mouse cardiac tissue was homogenized with 10 volumes of methanol containing L-2-chlorophenylalanine (50 ng/mL) as the internal standard using a tissue homogenizer. The homogenate was sonicated in an ice-water bath for 15 min, vortex-mixed for 2 min, and stored at −20 °C for 30 min to facilitate protein precipitation. After centrifugation at 14000 rpm and 4 °C for 10 min, the supernatant was collected, evaporated to dryness under a nitrogen stream, reconstituted in 150 μL of 50% methanol, and centrifuged again under the same conditions. The final supernatant was subjected to UHPLC-MS/MS analysis. A quality control (QC) sample was prepared by pooling equal volumes (10 μL) of supernatant from each sample. Chromatographic separation was performed on a Vanquish Horizon UHPLC system equipped with a Hypersil Gold C18 column (2.1 mm × 150 mm, 1.9 μm). Mobile phases consisted of 0.1% formic acid in acetonitrile (A) and 0.1% formic acid in water (B). The gradient elution profile was as follows: 98% B at 0–3 min, 98–30% B at 3–6 min, 30–0% B at 6–17 min, 0% B at 17–19 min, 0–98% B at 19–19.5 min, and 98% B at 19.5–21 min. The flow rate was 0.3 mL/min, the column temperature was maintained at 40 °C, and the injection volume was 5 μL.

Mass spectra were acquired using a Q-Exactive Plus mass spectrometer equipped with an

electrospray ionization (ESI) source operated in both positive and negative ion modes with full MS/ddMS^2 acquisition. The spray voltage was set at 3.5 kV in positive ion mode and 3.0 kV in negative ion mode. The vaporizer temperature was maintained at 350 °C. The sheath gas flow rate was set at 40 arb in positive ion mode and 38 arb in negative ion mode, while the auxiliary gas flow rate was maintained at 10 arb. The capillary temperature was set at 320 °C. The mass range was m/z 100–1 500. Full MS and MS/MS resolutions were set at 70 000 and 15 000, respectively. Stepped normalized collision energies (NCEs) were set at 20, 40, and 60. Raw data were processed by Compound Discoverer 3.2 to generate a data matrix. Multivariate statistics were performed with SIMCA 14.1 and MetaboAnalyst 6.0.

2.9 Spatial metabolomics analysis of cardiac tissues

After removal of surface blood residues and ventricular cavity contents, hearts were wrapped in aluminum foil and immediately snap-frozen in liquid nitrogen. Frozen cardiac sections (12 μm thick) were prepared using a cryostat microtome. Spatial metabolic profiling was performed using an AFADESI-MSI platform coupled with a Q-OT-qIT hybrid mass spectrometer. The spray solvent was 80% acetonitrile, which was delivered at a flow rate of 0.005 mL/min. The capillary temperature was set at 350 °C. The spray voltage was 4.5 kV, the spray pressure was 0.65 MPa, and the pumping gas flow rate was 80 L/min. The mass scan range was set at m/z 80–1 000, with an automatic gain control (AGC) target of 3×10^6. The spatial scanning step was set at 0.1 mm, and the mass resolution was 70 000 at m/z 200. MSI acquisition was performed continuously with a scanning speed of 0.2 mm/s along the x-axis and a stage movement speed of 0.2 mm/s along the y-axis. All raw data were converted and processed using Thermo File Converter and MassImager software, respectively.

2.10 Serum components analysis

Pooled drug-containing serum and blank serum samples were prepared by mixing equal volumes (0.5 mL) of serum collected from the treatment and model groups, respectively. Aliquots of pooled serum samples (100 μL drug-containing serum and 300 μL blank serum) were precipitated with four volumes of methanol-acetonitrile (1:1, v/v). After vortex mixing for 3 min and ultrasonication for 15 min, samples were centrifuged at 14 000 rpm for 10 min. The supernatants were evaporated to dryness under a nitrogen stream at 37 °C. The residues were reconstituted in methanol-acetonitrile

(1:1, v/v), centrifuged, and subjected to UHPLC-Q Exactive Plus MS analysis.

Chromatographic separation was performed on a Hypersil Gold C18 column (2.1 × 150 mm, 1.9 μm) using mobile phases consisting of 0.1% formic acid in acetonitrile (A) and 0.1% formic acid in water (B). The gradient elution profile was as follows: 98–75% B at 0–4 min, 75% B at 4–14 min, 75–70% B at 14–17 min, 70–2% B at 17–22 min, 2% B at 22–24 min, 2–98% B at 24–24.5 min, and 98% B at 24.5–27 min. The flow rate was 0.25 mL/min, the column temperature was maintained at 40 °C, and the injection volume was 5 μL. The mass spectrometry parameters were identical to those described for the untargeted metabolomics analysis. The acquired spectra were matched against databases and published literature using Xcalibur software, and compound identities were further confirmed using authentic standards.

2.11 Network pharmacology analysis based on serum-absorbed components

An internal library of CMW-derived serum-absorbed components was established based on the identification results obtained by UHPLC-Q Exactive Plus MS. Target prediction and database screening were subsequently performed to identify potential therapeutic targets of CMW-derived components and AMI-associated targets. After integrating target information and removing duplicate targets, a Venn diagram was generated to identify overlapping targets. The intersection targets were submitted to the STRING database for protein-protein interaction (PPI) network analysis, and the resulting network data were imported into Cytoscape for visualization. Gene Ontology (GO) enrichment and Kyoto Encyclopedia of Genes and Genomes (KEGG) pathway enrichment analyses of the intersection targets were performed using Metascape.

2.12 RT-qPCR analysis

Total RNA was extracted from mouse cardiac tissues using the Eastep® Super Total RNA Extraction Kit . The extracted RNA was reverse-transcribed into complementary DNA (cDNA) using a Prime Scrip™ RT Master Mix. Gene expression analysis was conducted with the TB Green® Premix Ex Taq™ II. Data were analyzed using the relative quantification method, specifically the ΔΔCt method. For each sample, the mean Ct value was calculated, and relative mRNA expression levels were determined using the $2^{-\Delta\Delta Ct}$ method. The primer sequences employed in this study are presented in Table 1.

Table 1 Primers sequences in Mouse cardiac tissues

Genes	Forward	Reverse
LPCAT	CCTGTATGCCAGCAATGTGAGG-3	TCAGCAGGCAAGCGAAGTTGTC
PLA2	CTGTCAGATGCACGACCGTTGT	GAGCCTCATTGGACAGAAGGAG
GPAT	GCAAGCACTGTTACCAGCGATC	TGCAATCAGCCTTCGTCGGAAG-3
Lipin1	TAAACGGAGCCGACACCTTGGA	CCGTTGTCACTGGCTTGTTTGG
CCTα	TCCTTCCAAAGTGCAGCGTTGC	GCAGGCTTCTTCCATAGTCACC
vinculin	CAGCCCAGATGCTTCAGTCA	CGAACCTCAGCCTCATCGAA
SRC	ACTGCCTCTCTGTATCCGACT	TGTAGAAACCGCCGCTGTCCA
PI3K	GTCCGTCCTGGAGAACTTGG	TGAGGCGTTTCTGGATTGC
AKT	CGCCTGCCCTTCTACAACCAG	GCATGATCTCCTTGGCATCCTC
Bax	GCTGGACATTGGACTTCCTC	CTCAGCCCATCTTCTTCCAG
Bcl-2	GCTGGGGATGACTTCTCTCG	CATGACCCCACCGAACTCAA
vinculin	CAGCCCAGATGCTTCAGTCA	CGAACCTCAGCCTCATCGAA
SRC	ACTGCCTCTCTGTATCCGACT	TGTAGAAACCGCCGCTGTCCA

2.13 Western blot analysis

Mouse cardiac tissues were homogenized in lysis buffer using a tissue homogenizer. The supernatant was centrifuged, and the total protein concentration was determined using a BCA protein assay kit. The protein sample was mixed with protein loading buffer and heated at 100 °C for 10 min. Proteins were separated by sodium dodecyl sulfate–polyacrylamide gel electrophoresis.

The proteins were transferred onto PVDF membranes, which were blocked and incubated. overnight at 4 °C with primary antibodies against p-SRC, SRC, p-PI3K, PI3K, p-AKT, AKT, Bcl-2, and Bax. The following day, secondary antibodies were incubated at room temperature, and ECL development was performed. The grayscale values of each protein band were analyzed using ImageJ software. The relative expression levels of the target proteins were calculated using vinculin as an internal control.

2.14 Immunohistochemical analysis

Immunohistochemical staining for p-SRC, SRC, p-PI3K, PI3K, p-AKT, AKT, Bcl-2, and Bax was performed according to standard procedures. Sections of mouse cardiac tissues were baked, deparaffinized in xylene, and hydrated in graded alcohols. The sections were then treated with 3% H_2O_2 to quench endogenous peroxidase activity. An appropriate amount of the corresponding primary antibody was added to each section and incubated for 30 min. After washing with PBST, a

peroxidase-labeled sheep anti-mouse/rabbit IgG polymer was added to each section and incubated at room temperature for 1 h. Sections were developed using freshly prepared 3,3′-diaminobenzidine (DAB) chromogen solution. Positive cells were determined by measuring the integrated optical density using ImageJ.

2.15 Statistical analysis

The results are expressed as the mean ± standard deviation (mean ± SD). Comparisons between two groups were performed using Student's t-test, whereas comparisons among multiple groups were assessed by analysis of variance (ANOVA) using GraphPad Prism 8.0. A *p*-value of less than 0.05 was considered indicative of statistical significance.

3 Results

3.1 CMW ameliorates myocardial injury in AMI mice

After LAD coronary artery ligation, mice in the MOD group exhibited marked electrocardiographic abnormalities, including ST-segment elevation, baseline drift, and reduced QRS complex amplitude, indicating successful establishment of the AMI model (Fig. 1B). In contrast, treatment with Compound Danshen Dripping Pill or CMW partially restored the ECG patterns, as evidenced by reduced ST-segment elevation, improved baseline stability, and increased QRS complex amplitude. H&E staining revealed disrupted myocardial fibers, nuclear pyknosis, cytoplasmic lysis, extensive myocardial necrosis, inflammatory cell infiltration, and fibrous hyperplasia in cardiac tissues from MOD mice (Fig. 1C). CMW treatment markedly alleviated these pathological changes, with effects comparable to those observed in the CDDP group.

Evans Blue-TTC double staining showed extensive infarct areas in MOD mice, accompanied by a significantly increased infarct size ($P < 0.001$; Fig. 2A). After CMW administration, infarct size was significantly reduced ($P < 0.001$), with the infarct area decreased by more than 50%. Serum biochemical analysis showed that the levels of myocardial injury markers, including cTnI, BNP, CK-MB, and LDH, were significantly increased in MOD mice ($P < 0.001$; Fig. 2 B–E). Treatment with Compound Danshen Dripping Pill or CMW significantly reduced the levels of these biomarkers to varying degrees ($P < 0.001$; Fig. 2 B–E).

Treatment with Compound Danshen Dripping Pill or CMW reduced the levels of these efficacy indicators to different extents ($P < 0.001$), and CMW showed greater reductions in the measured indicators. Collectively, these results indicated that CMW ameliorated LAD coronary artery ligation-induced myocardial injury by improving electrocardiogram abnormalities, reducing myocardial pathological damage, decreasing infarct size, and lowering circulating myocardial injury biomarkers.

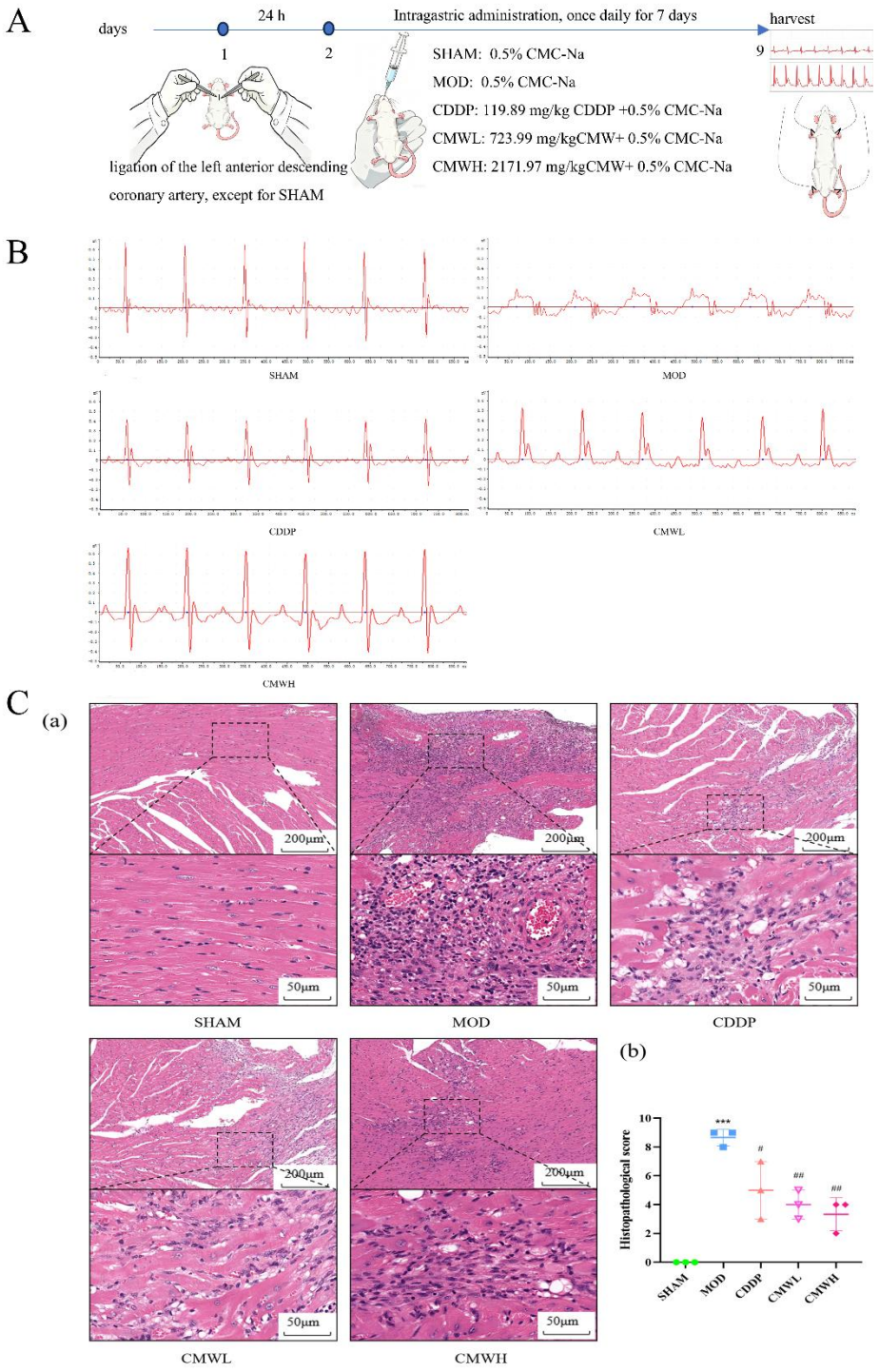


Fig. 1 CMW ameliorates electrocardiographic abnormalities and myocardial histopathological injury in AMI mice. **A** Schematic diagram of the experimental protocol. **B** Representative electrocardiogram traces of mice from each group, $n = 3$. **C** Representative images and scoring of cardiac histopathology in mice, $n = 3$. (a) Representative H&E staining images of cardiac tissues, (b) Semi-quantitative histopathological injury score of myocardium. Compared with the SHAM group, $^{***}P < 0.001$. Compared with the MOD group, $^{\#}P < 0.05$, $^{\#\#}P < 0.01$, and $^{\#\#\#}P < 0.001$.

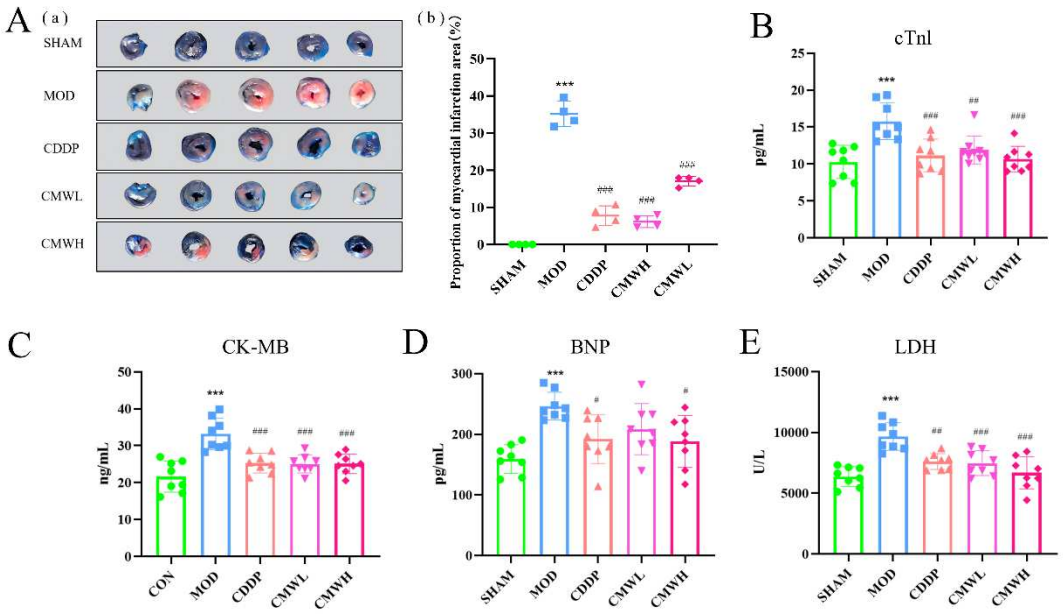


Fig. 2 CMW reduces myocardial infarct size and decreases serum myocardial injury biomarkers in AMI mice. **A** Representative images of infarct size in mouse cardiac tissue and statistical chart of infarct size ratio in each group, $n = 4$. (a) Representative Evans blue-TTC double staining images of mouse hearts, (b) Statistical histogram of myocardial infarct area percentage. **B–E** Serum levels of myocardial injury biomarkers cTnI, BNP, CK-MB and LDH, $n = 8$. Compared with the SHAM group, $^{***}P < 0.001$. Compared with the MOD group, $^{\#}P < 0.05$, $^{\#\#}P < 0.01$, and $^{\#\#\#}P < 0.001$.

3.2 CMW reshapes myocardial endogenous metabolic profiles and restores disordered lipid metabolism in AMI mice

Because myocardial ischemia and metabolic disturbance are closely linked in AMI, untargeted metabolomic analysis of cardiac tissues was performed to evaluate the metabolic effects of CMWH. Quality control assessments showed that QC samples clustered tightly in the PCA score plot (Fig. 3A-a), all Hotelling's T^2 values fell within the 95% confidence interval (Fig. 3A-b), more than 90% of variables showed RSD values ≤30% (Fig. 3A-c), and the top 10 chromatographic peaks exhibited RSD values <15% (Fig. 3A-d), indicating satisfactory stability and reproducibility of the analytical platform. Overlay of total ion chromatograms from six QC samples under both ESI^+ and ESI^- modes further demonstrated high consistency in peak profiles and retention times (Fig. 3A-e, f).

Multivariate statistical analysis revealed clear separation among the SHAM, MOD, and CMWH groups. PCA and OPLS-DA score plots showed tight intra-group clustering and distinct

inter-group discrimination (Fig. 3B-a, b). Compared with the SHAM group, the MOD group exhibited a marked metabolic shift, indicating substantial metabolic alterations following AMI induction. The CMWH group was distinguished from the MOD group, indicating that CMWH remodeled the cardiac metabolome in AMI mice. OPLS-DA models constructed for SHAM versus MOD and MOD versus CMWH both showed clear separation between groups (Fig. 3B-c, e), and 200-cycle permutation tests verified that neither model was overfitted (Fig. 3B-d, f), supporting robust model validity.

Volcano plot analysis was performed to identify differential metabolites between the MOD and SHAM groups (Fig. 3C) and between the CMWH and MOD groups (Fig. 3D). Using criteria of $P < 0.05$ and fold change ≥ 1.2 or ≤ 0.83, 44 reversed differential metabolites were identified after CMWH administration. Hierarchical clustering of these metabolites showed that the MOD group had a distinct metabolic profile from SHAM, whereas the CMWH group clustered more closely with SHAM (Fig. 3E), suggesting that CMWH restored metabolic patterns toward normal. KEGG enrichment analysis further highlighted 19 altered pathways, of which seven were significantly regulated ($P < 0.05$), including pantothenate and CoA biosynthesis, phenylalanine metabolism, taurine and hypotaurine metabolism, glycerophospholipid metabolism, pyrimidine metabolism, β-alanine metabolism, and phenylalanine, tyrosine, and tryptophan biosynthesis (Fig. 3F).

Given that lipid metabolism disorder is a key pathological mechanism in AMI, and that glycerophospholipids serve as essential structural components of cellular and organelle membranes, glycerophospholipid metabolism was further investigated[19, 20]. Myocardial ischemia and hypoxia can disrupt membrane integrity through alterations in glycerophospholipid metabolism, which may contribute to cellular damage, apoptosis, and necrosis[21]. The enrichment of glycerophospholipid metabolism suggested that this pathway may represent a metabolic signature associated with AMI progression and CMWH treatment.

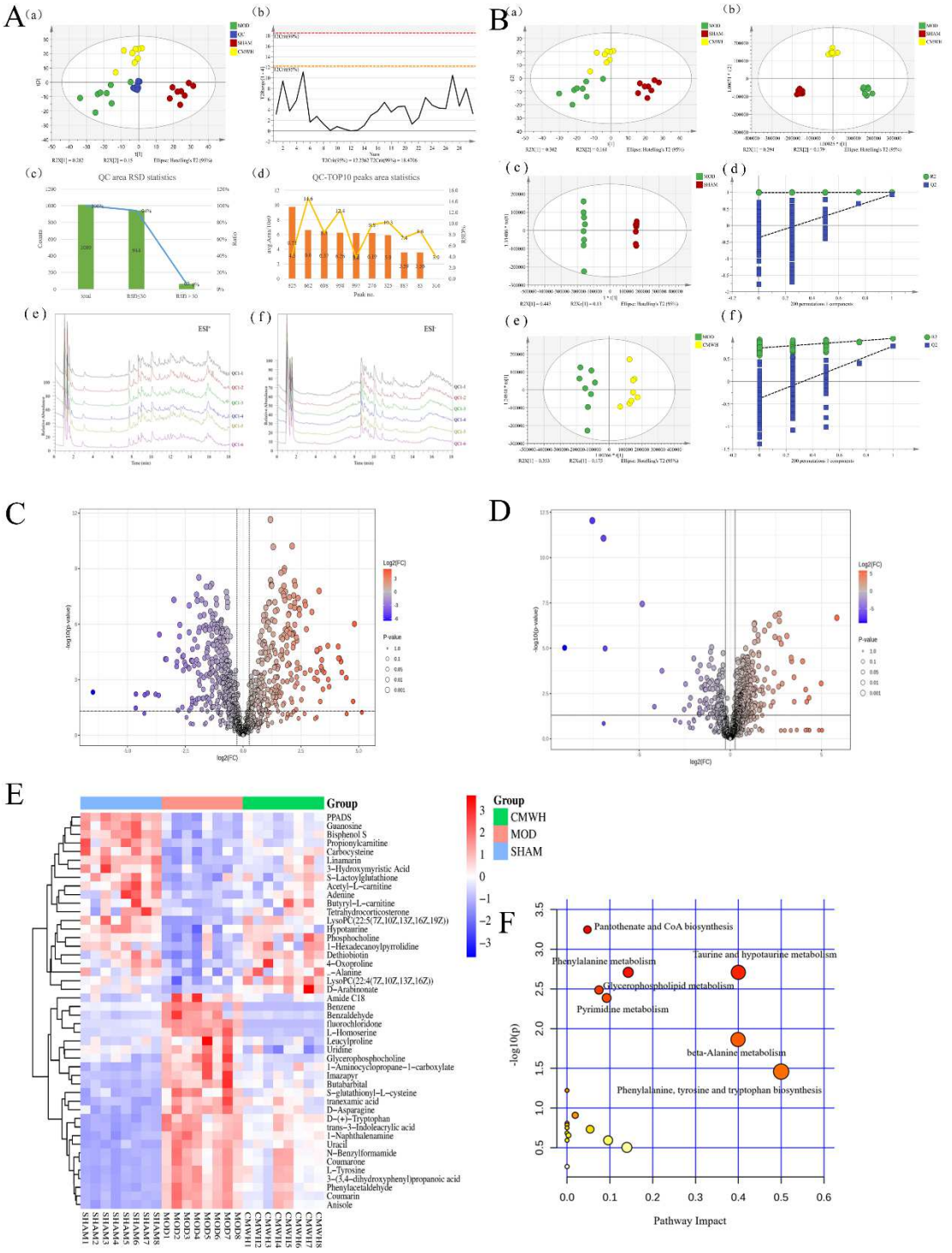


Fig. 3 Metabolomics profiling and differential metabolic pathway analysis of cardiac tissues from AMI mice. **A** Quality control. (a) Overall distribution of all samples, (b) Linear plot of Hotelling's T2 Range, (c) Statistical histogram of RSD% for all peak areas of QC samples. (d) Peak areas and corresponding RSD% of the top 10 peaks in QC samples, (e–f) Overlay chromatograms of all QC samples under ESI^+ and ESI- mode. **B** Multivariate statistical analysis of cardiac metabolome, (a) PCA score plot, (b) OPLS-DA score plot of sample, (c–d) OPLS-DA analysis

of SHAM and MOD groups, (e–f) OPLS-DA analysis of MOD and CMWH groups. **C** Volcano plot showing differentially expressed metabolites between the MOD and SHAM groups. **D** Volcano plot showing differentially expressed metabolites between the CMWH and MOD groups. **E** Heatmap visualization of all identified differential metabolites. **F** Bubble diagram of enriched differential metabolic pathways.

3.3 CMW restores spatial metabolic alterations and regulates glycerophospholipid metabolism-associated enzymes in AMI mice

To further characterize the spatial heterogeneity of glycerophospholipid metabolic alterations beyond bulk metabolomic profiling, spatial metabolic mapping was performed using mass spectrometry imaging (MSI). Thermo File Converter software was used to generate theoretical m/z values for target metabolites under positive and negative ESI conditions, including phosphatidylcholine (PC, $[M+H]^+$, m/z 758.5695), phosphocholine (PCho, $[M+H]^+$, m/z 184.0733), glycerophosphocholine (GPC, $[M+H]^+$, m/z 258.1101), lysophosphatidylcholine 22:5 (LPC 22:5, $[M+H]^+$, m/z 570.3554), lysophosphatidylcholine 16:0 (LPC 16:0, $[M+H]^+$, m/z 496.3398), phosphatidylserine (PS, $[M-H]^-$, m/z 790.5604), and phosphatidic acid (PA, $[M-H]^-$, m/z 747.4970).

The MSI maps revealed region-specific spatial distributions of glycerophospholipid metabolites in the myocardium of the MOD group, particularly for PCho, LPC (22:5), and GPC. The overall spatial distribution patterns of these metabolites are shown that distinct signal intensities of small molecules including PCho, LPC (22:5) and GPC were detected between infarcted and non-infarcted myocardial regions in the MOD group. After CMWH administration, such interregional signal differences were attenuated, and the metabolite distribution pattern was close to that of the SHAM group (Fig. 4A-a). Quantitative analysis of normalized metabolite signal intensities showed that, compared with the SHAM group, the cardiac abundance of PC, PCho, LPC (22:5), PS and PA decreased, while the levels of GPC and LPC (16:0) increased in MOD mice, significant intergroup differences were observed for PCho, LPC (22:5), GPC and PS ($P < 0.05$). Following CMWH treatment, the levels of these dysregulated metabolites generally showed a restoration trend, with PCho, LPC (22:5), and GPC showing significant recovery compared with the MOD group ($P < 0.05$). These MSI data indicated disrupted glycerophospholipid metabolism in AMI myocardium, and CMWH may regulate this metabolic pathway by altering the tissue distribution of PCho, LPC (22:5) and GPC (Fig. 4A-b).

Subsequently, the peak areas of three differential metabolites identified by untargeted metabolomics analysis, namely PCho, LPC (22:5), and GPC, were further quantified (Fig. 4B–D). Compared with the SHAM group, the levels of PCho and LPC (22:5) were significantly decreased ($P < 0.01$), whereas the level of GPC was significantly increased ($P < 0.001$) in the MOD group. After CMW treatment, these changes exhibited a partial reversal tendency. The consistency between MSI imaging and untargeted metabolomics results further supported the involvement of glycerophospholipid metabolic remodeling in the cardioprotective effects of CMW.

RT-qPCR was performed to determine the myocardial mRNA expression of key genes involved in glycerophospholipid metabolism, including PLA2, LPCAT, TTCα, Lipin1, and GPAT (Fig. 4E–I). Compared with the SHAM group, MOD mice showed increased mRNA expression of PLA2 and TTCα but decreased expression of LPCAT, Lipin1, and GPAT ($P < 0.05$, $P < 0.01$). CMWH intervention remarkably reversed the abnormal mRNA expression of PLA2, TTCα, LPCAT, Lipin1 and GPAT ($P < 0.05$). Taken together, CMWH exerts anti-AMI effects by modulating the expression of PLA2, TTCα, LPCAT, Lipin1 and GPAT to restore disordered glycerophospholipid metabolism.

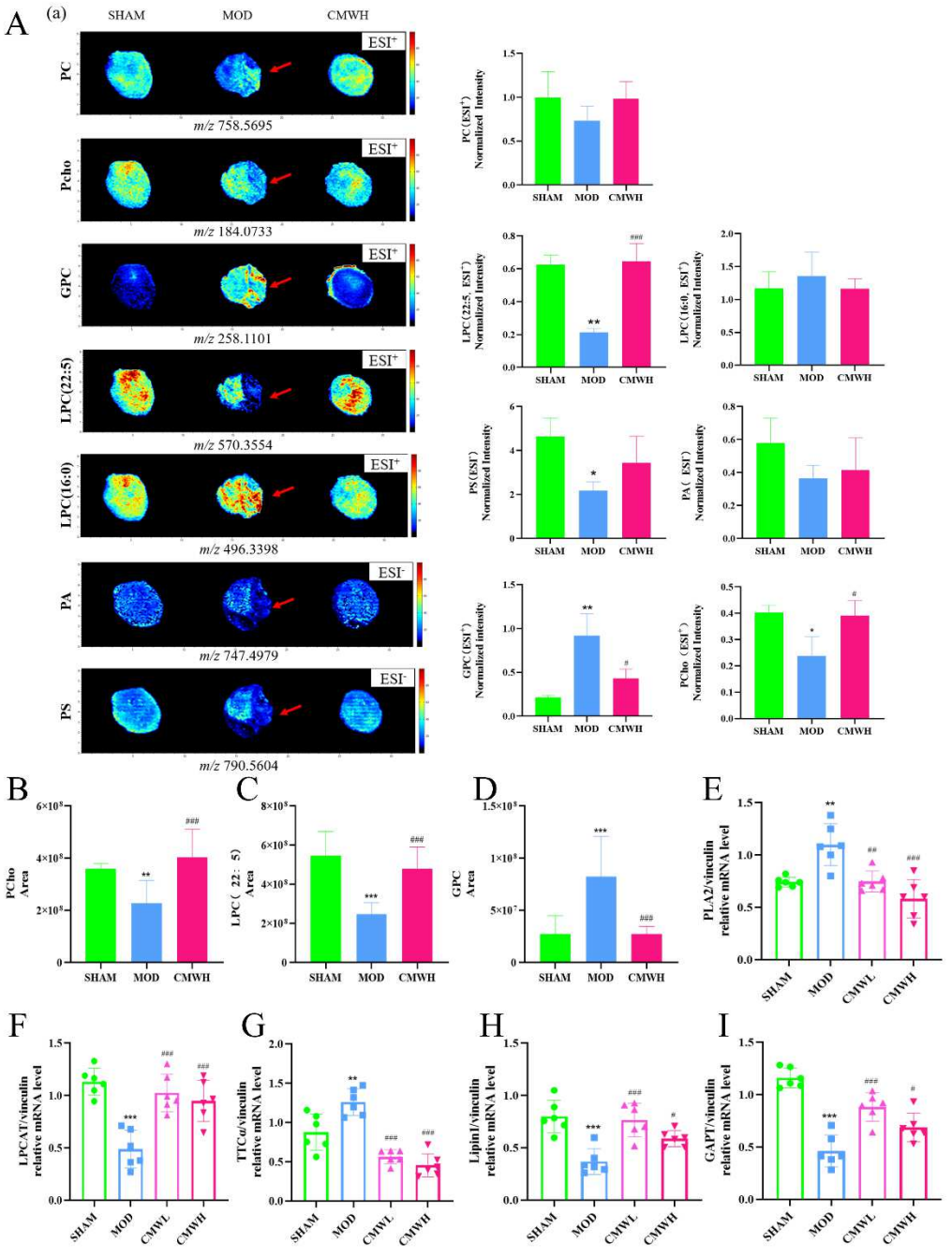


Fig. 4 CMWH modulates glycerophospholipid metabolism and related gene expression in the infarcted myocardium of AMI mice. **A** Distribution of key metabolites in mouse cardiac tissues in different groups, $n = 3$. (a) MS imaging maps of key glycerophospholipid metabolites in cardiac, (b) Quantitative statistical histogram of normalized signal intensity for each metabolite. **B**–**D** Peak area quantification histograms of PCho, LPC (22:5) and GPC metabolites, $n = 8$. **E**–**I** Relative mRNA expression levels of glycerophospholipid metabolism-related genes (PLA2, LPCAT, TTC4, Lipin, GAPT) normalized to vinculin, $n = 8$. Compared with the SHAM group, $^{*}P < 0.05$,$^{**}P < 0.01$,$^{***}P < 0.001$. Compared with the MOD group, $^{\#}P < 0.05$, $^{\#\#}P < 0.01$, and $^{\#\#\#}P < 0.001$.

3.4 Identification of CMW-derived components in the serum of AMI mice

Based on previous chemical identification data of CMW from our research group, combined with a data processing using Compound Discoverer 3.2 software, serum-absorbed constituents were identified. The identification results revealed a total of 26 serum-absorbed components in AMI mice treated with CMW, which were classified into flavonoids, alkaloids, organic acids and phenylpropanoids (Table 2).

Table 2 Serum components profiling of CMW in AMI mice

No.	Compound	Formula	Retention time/min	ppm	MS^1	Adduct form	MS^2	Class
1	2-Hydroxycinnamic acid	$C_9H_8O_3$	7.93	−4.97	163.04006	$[M-H]^-$	119.04898	Phenylpropanoids
2	Magnoflorine	$C_{20}H_{23}NO_4$	6.23	−4.84	342.16998	$[M+H]^+$	297.11172,265.08554,237.09067	Alkaloids
3	Melilotoside	$C_{15}H_{18}O_8$	4.93	1.51	325.09289	$[M-H]^-$	163.03905,119.04897	Phenylpropanoids
4	Syringacetone	$C_{10}H_{12}O_4$	7.75	−1.57	197.08083	$[M+H]^+$	173.08038,155.07016,140.04662	Phenylpropanoids
5	3-Hydroxy-2-methylpyridine	C_6H_7NO	4.24	2.83	110.06004	$[M+H]^+$	83.04984,82.06587,67.05504,55.05511	Alkaloids
6	3-Hydroxy-2-pyridinecarboxylic acid	$C_6H_5NO_3$	2.32	−1.19	140.03421	$[M+H]^+$	122.02396,113.04296,112.03960	Other compounds
7	Anisaldehyde	$C_8H_8O_2$	7.20	−3.07	137.05970	$[M+H]^+$	122.03629,109.06491,94.04173	Phenylpropanoids
8	Caffeic acid	$C_9H_8O_4$	7.67	−2.95	179.03498	$[M-H]^-$	135.04387,107.04891,93.03315	Phenylpropanoids
9	Coniferin	$C_{16}H_{22}O_8$	8.43	0.43	341.12419	$[M-H]^-$	179.07033，164.04674	Phenylpropanoids
10	Quinic acid	$C_7H_{12}O_6$	1.66	−3.28	191.05611	$[M-H]^-$	173.04469,127.03893,93.03333,85.02824	Organic acids
11	Ligustilide	$C_{12}H_{14}O_2$	22.42	−0.28	191.10665	$[M+H]^+$	163.11172,145.10121,117.07004	Phenylpropanoids
12	Naringenin chalcone	$C_{15}H_{12}O_5$	7.79	–2.36	273.07575	$[M+H]^+$	171.02864,153.01816,147.04390,119.04937	Flavonoids
13	Norboldine	$C_{18}H_{19}NO_4$	5.64	−1.9	314.13868	$[M+H]^+$	297.11166,282.08786,265.08548,273.09032	Alkaloids
14	Quercitrin	$C_{21}H_{20}O_{11}$	8.31	1.03	447.09328	$[M-H]^-$	271.06152,151.00276	Flavonoids
15	Salicylic acid	$C_7H_6O_3$	9.62	−7.63	137.02441	$[M-H]^-$	93.03315	Organic acids
16	Salidroside	$C_{14}H_{20}O_7$	5.08	-0.88	299.11362	$[M-H]^-$	119.04881,113.02308,101.02303,89.02304	Phenylpropanoids
17	Norsalsolinol	$C_{10}H_{13}NO_2$	1.75	−1.25	180.10190	$[M+H]^+$	163.07521,145.06471,137.05966,117.07005	Alkaloids
18	Sedanolide	$C_{12}H_{18}O_2$	10.07	−1.69	195.13795	$[M+H]^+$	177.12706,159.11658,133.10101,121.06481, 119.08558	Terpenoids
19	Shikimic acid	$C_7H_{10}O_5$	1.74	−5.42	173.04554	$[M-H]^-$	154.99767,111.00758,93.03333,85.02824	Organic acids

No.	Compound	Formula	Retention time/min	ppm	MS^1	Adduct form	MS^2	Class
20	Sinapic acid	$C_{11}H_{12}O_5$	5.48	−1.23	225.07575	$[M+H]^+$	207.06499,175.03882,147.04393,119.04929, 91.05467	Phenylpropanoids
21	Trigonelline	$C_7H_7NO_2$	1.64	−1.46	138.05495	$[M+H]^+$	110.06048,94.06570,92.05009,67.05508	Alkaloids
22	Fraxinon	$C_{14}H_{16}O_3$	22.21	−1.41	233.11722	$[M+H]^+$	215.14316,131.08568	Terpenoids
23	Chlorogenic acid	$C_{16}H_{18}O_9$	5.58	1.27	353.08780	$[M-H]^-$	191.05516,161.02344,127.03850,85.02808	Organic acids
24	Naringin	$C_{27}H_{32}O_{14}$	7.79	−0.5	579.17192	$[M-H]^-$	459.11493,271.06085,151.00244,119.04887	Flavonoids
25	Afzeliin	$C_{21}H_{20}O_{10}$	8.74	0.73	431.09837	$[M-H]^-$	285.07986,284.03217,255.02945,227.03423	Flavonoids
26	Neochlorogenic acid	$C_{16}H_{18}O_9$	4.86	1.33	353.08780	$[M-H]^-$	191.05551,179.03427,173.04489,135.04413	Organic acids

3.5 Network pharmacology analysis of CMW in the treatment of AMI based on serum-absorbed components

The intersection analysis between 26 serum-absorbed components and AMI-associated targets identified 227 overlapping targets (Fig. 5A). Using a degree score >6.7 as the selection threshold, 62 hub targets were identified from the PPI network, with SRC showing the highest connectivity among these hub targets (Fig. 5B). Pathway enrichment analysis revealed that these 62 hub targets were primarily enriched in the Rap1, HIF-1, VEGF, and PI3K/AKT signaling pathways (Fig. 5C–D). Previous studies have suggested that PI3K/AKT pathway modulation may alleviate glycerophospholipid metabolic disorders, reduce myocardial lipid accumulation, and regulate fatty acid metabolism in myocardial fibrosis models[22]. Moreover, this pathway serves as a hub for maintaining lipid metabolic homeostasis and regulating inflammatory responses[23], suggesting that the PI3K/AKT signaling pathway may represent the core pathway underlying the therapeutic effect of CMW against AMI.

Subsequently, molecular docking analysis was performed between the serum-absorbed components and the five top-ranked hub targets, and a binding-energy heatmap was generated (Fig. 5E). Generally, binding energies ≤−1.2 kcal/mol were considered indicative of favorable interactions, whereas values ≤−5 kcal/mol and ≤−7 kcal/mol represented stronger and strong binding affinities, respectively. SRC (PDB ID: 1A07), PIK3CA (PDB ID: 4JPS), STAT3 (PDB ID: 6NJS), PIK3R1 (PDB ID: 7PG6), and AKT1 (PDB ID: 4EJN) exhibited favorable binding affinities with the 26 serum-absorbed components, with binding energies below −1.2 kcal/mol. In particular, SRC, PIK3R1, and AKT1 displayed stronger predicted interactions with these components, suggesting that they may serve as candidate targets involved in the pharmacological effects of CMW.

The three components with the lowest binding energies for SRC, PIK3R1 and AKT1 were selected for conformational visualization using PyMOL (Fig. 5F). SRC bound to chlorogenic acid, neochlorogenic acid and naringin via salt bridges, hydrogen bonds and hydrophobic interactions. AKT1 interacted with afzelin, quercitrin and naringin mainly through hydrogen bonds and hydrophobic interactions, and additional π-stacking interactions were observed for afzelin and quercitrin. For PIK3R1, hydrogen bonds and hydrophobic interactions were detected with afzelin, norboldine and naringin; a salt bridge was formed with naringin, whereas π-stacking occurred with afzelin and norboldine. Integrating pathway enrichment and molecular docking results, these

findings suggest that the PI3K/AKT signaling pathway may represent a potential signaling axis involved in the cardioprotective effects of CMW, with SRC identified as a candidate hub target.

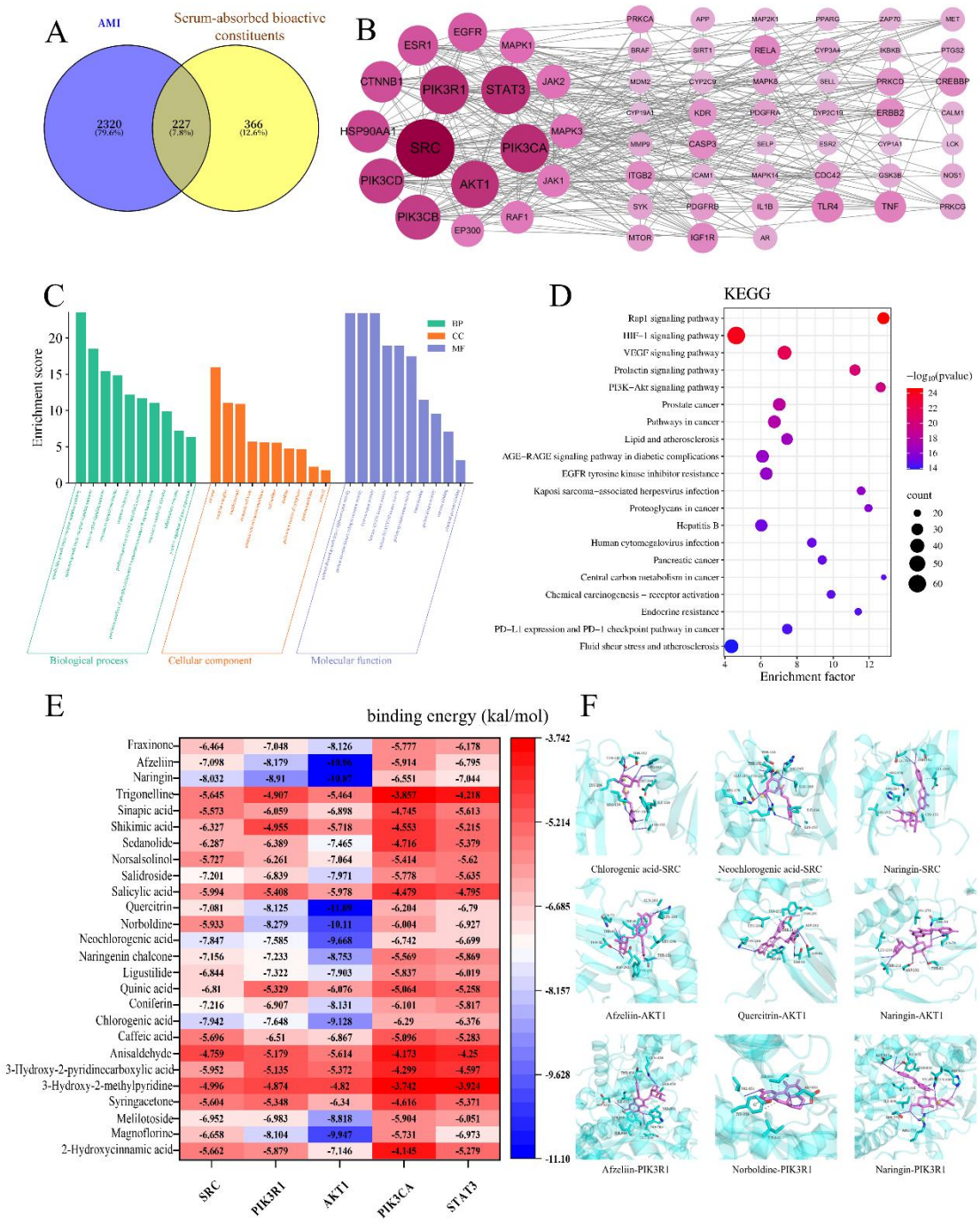


Fig. 5 Network pharmacology and molecular docking analyses of CMW for AMI treatment. **A** Venn diagram showing the intersection targets of AMI disease targets and targets of serum-absorbed bioactive constituents. **B** Protein-protein interaction (PPI) network of overlapping core targets. **C** GO enrichment bar chart of core targets, including Biological Process (BP), Cellular Component (CC), and Molecular Function (MF). **D** KEGG pathway enrichment bubble plot of core therapeutic targets. **E** Heatmap of molecular docking binding energies (kcal/mol)

between 26 serum-absorbed components and five hub proteins (SRC, PIK3R1, AKT1, PIK3CA, STAT3). **F** Representative 3D binding conformation visualization of ligand-protein complexes generated by PyMOL.

3.6 CMW activates the SRC/PI3K/AKT signaling pathway and alleviates apoptosis-associated changes in AMI mice

RT-qPCR was performed to evaluate the transcriptional expression levels of SRC, PI3K, AKT, Bax, and Bcl-2 in cardiac tissues. Compared with the SHAM group, the MOD group exhibited decreased mRNA expression of SRC, PI3K, AKT and Bcl-2, along with increased Bax mRNA level. CMW treatment effectively upregulated the mRNA expression of SRC, PI3K, AKT and Bcl-2, while downregulating Bax mRNA expression (Fig. 6A–E). Western blot further detected the corresponding protein expression and phosphorylation levels. Consistently, the MOD group showed reduced ratios of p-SRC/SRC, p-PI3K/PI3K, p-AKT/AKT and lower Bcl-2 protein expression, whereas Bax protein was upregulated (Fig. 6F). These abnormal protein changes were significantly reversed after CMW intervention. Immunohistochemical analysis further verified the above protein expression trends (Fig. 6G). These findings suggest that CMW activates the SRC/PI3K/AKT signaling pathway and modulates the expression of the apoptosis-related proteins Bcl-2 and Bax, which may contribute to its cardioprotective effects against AMI injury in mice.

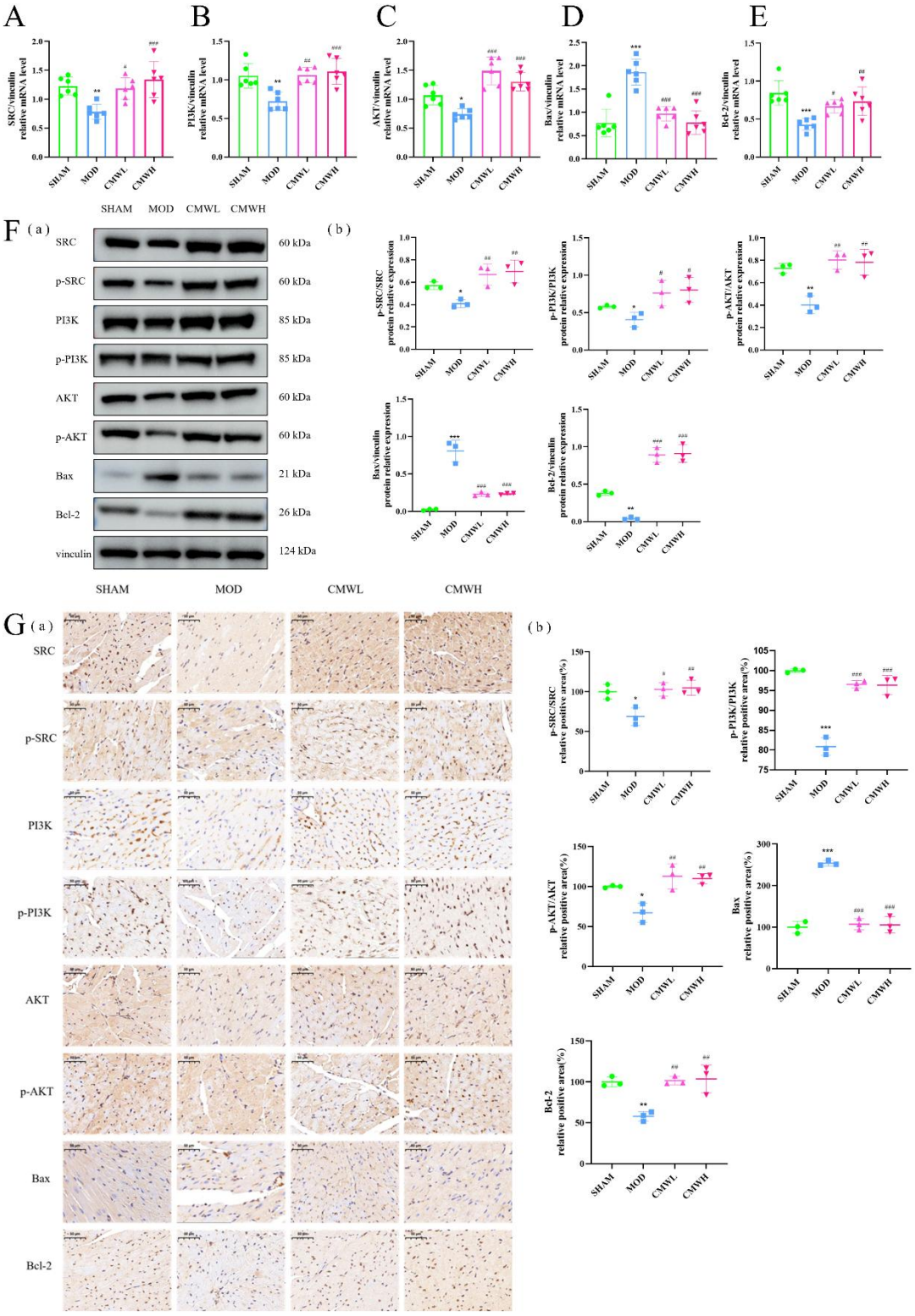


Fig. 6 CMW activates the SRC/PI3K/AKT signaling pathway and regulates apoptosis-related molecules in myocardial tissue of AMI mice. **A**–**E** Relative mRNA expression levels of SRC, PI3K, AKT, Bax and Bcl-2 normalized to vinculin, n = 6. **F** Representative western blot bands, n = 3. (a) and quantitative analysis (b) of p-SRC, SRC, p-PI3K, PI3K, p-AKT, AKT, Bax and Bcl-2 protein levels. **G** Immunohistochemical staining images (a) and

quantitative statistics of positive area ratio (b) for SRC, p-SRC, PI3K, p-PI3K, AKT, p-AKT, Bax and Bcl-2 in cardiac tissues. Compared with the SHAM group, $^{*}P < 0.05$,$^{**}P < 0.01$,$^{***}P < 0.001$. Compared with the MOD group, $^{\#}P < 0.05$, $^{\#\#}P < 0.01$, and $^{\#\#\#}P < 0.001$.

4 Discussion

AMI remains a major contributor to global cardiovascular morbidity and mortality[17, 24]. Owing to its complex pathological mechanisms, available pharmacological strategies for preventing myocardial injury and improving cardiac recovery remain limited, highlighting the need for novel therapeutic approaches. Traditional Chinese medicines (TCMs) have attracted increasing attention in the management of myocardial infarction due to their multi-component and multi-target characteristics, demonstrating growing application potential in preoperative intervention, integrated Chinese and Western medicine treatment after surgery, early rehabilitation, and long-term prognosis improvement[25]. Among these medicines, *Cinnamomum migao*, a traditional medicinal plant commonly used for the treatment of cardiovascular diseases in Southwest China, has been traditionally administered in the form of decoctions. Its cardioprotective effects and underlying mechanisms remain insufficiently characterized. In this study, the cardioprotective effects of the traditional decoction form of CMW against AMI injury were systematically investigated through pharmacological evaluation, metabolomics, spatial metabolic imaging, and molecular validation.

To elucidate the metabolic basis underlying the cardioprotective effects of CMW, an integrated strategy combining UHPLC-MS/MS-based untargeted metabolomics and AFADESI-MSI spatial metabolomics was employed in this study. Conventional metabolomics provides comprehensive information regarding metabolic alterations but lacks spatial resolution within tissues, whereas AFADESI-MSI further enables visualization of metabolite distribution across myocardial regions. Untargeted metabolomics analysis revealed that CMW treatment reversed multiple dysregulated metabolic pathways in AMI myocardial tissues, among which glycerophospholipid metabolism showed a prominent recovery pattern. Moreover, accumulating evidence has indicated that glycerophospholipid metabolism plays an important role in the progression of AMI[26]. Glycerophospholipid metabolism is markedly altered in myocardial tissue after infarction, and modulation of glycerophospholipid metabolic disturbances has been reported to alleviate cardiac

injury[19, 27]. Based on these findings, spatial metabolomics was further applied to investigate the distribution characteristics of key metabolites involved in glycerophospholipid metabolism within myocardial tissue, providing additional evidence for the importance of this metabolic pathway in AMI intervention.

Further spatial metabolomics analysis demonstrated that CMW treatment modulated the cardiac distribution of lipid molecules, including PC, PCho, GPC, LPC, PS, and PA. Among these metabolites, PC is the predominant glycerophospholipid component of cellular membranes, accounting for approximately 45%–55% of total phospholipids in mammalian cells[28], and has been proposed as a potential biomarker for cardiovascular diseases and post-myocardial infarction heart failure[29]. Hydrolysis of PC generates LPC, which participates in inflammatory responses and the development of atherosclerotic plaques and has been considered a potential therapeutic target for cardiovascular diseases[30]. PA serves not only as an important component of cellular membranes but also as an intracellular second messenger involved in the regulation of mitochondrial function and energy metabolism[31]. PCho is a direct precursor for PC synthesis through the Kennedy pathway, and its level has been reported to decrease significantly in myocardial injury models, which is consistent with the findings observed in AMI mice in the present study[32]. GPC, the terminal product generated from complete PC hydrolysis, exhibits cardioprotective activity and can alleviate cardiac functional impairment[33, 34]. PS is located on the inner leaflet of the cell membrane and contributes to the maintenance of membrane integrity and signal transduction. Exogenous PS supplementation has been reported to reduce infarct size and improve cardiac function in myocardial infarction models[35]. These findings suggest that, in addition to correcting global glycerophospholipid metabolic disturbances induced by AMI, CMW may alleviate myocardial ischemic injury by remodeling the spatial distribution of these lipid molecules and correcting metabolic abnormalities within infarct regions.

Notably, CMW regulated the expression of GPAT, CCTα, PLA2, LPCAT, and Lipin1 in AMI mice. These enzymes are key rate-limiting regulators involved in the Kennedy pathway and Lands cycle, which together constitute major pathways responsible for myocardial PC synthesis and remodeling. Among these enzymes, GPAT catalyzes the first rate-limiting step of glycerophospholipid synthesis, and its activity is suppressed under ischemic and hypoxic conditions, thereby contributing to cardiomyocyte injury and apoptosis[36]. Within the Kennedy pathway, CCTα

functions as the rate-limiting enzyme in the CDP-choline branch and directly determines the efficiency of PC synthesis[37]. The Lands cycle is responsible for phospholipid remodeling and repair, while LPCAT-mediated reacylation reactions within this cycle are essential for maintaining lipid homeostasis and cell survival[38]. Abnormal expression of Lipin1 and PLA2 can disrupt lipid metabolism and has been implicated in the pathological processes of lipid imbalance and cardiac hypertrophy, respectively[39]. Integrating the multi-omics findings, CMW may regulate myocardial PC metabolism through these enzymes, and that glycerophospholipid metabolic regulation may represent an important metabolic basis underlying the protective effects of CMW against AMI.

The PI3K/AKT signaling pathway serves as an important signaling hub that connects extracellular stimuli with intracellular responses[40]. SRC is a key upstream regulator of the PI3K/AKT pathway and can activate downstream PI3K/AKT signaling by promoting AKT phosphorylation[41]. The SRC/PI3K/AKT axis participates in AMI initiation, progression, and repair by regulating key pathological processes, including lipid metabolism and energy metabolic disturbances. It represents an important regulatory target in AMI-related myocardial injury and a major signaling pathway involved in cardioprotection by various interventions[42-47]. Moreover, this pathway regulates apoptosis by modulating the expression of downstream apoptosis-related factors[48, 49]. Cardiomyocyte apoptosis is a major manifestation of myocardial injury after AMI and contributes to infarct expansion and deterioration of cardiac function. As a central effector of the PI3K/AKT signaling axis, AKT is involved in various physiological and pathological processes, including cell proliferation, apoptosis, differentiation, and migration[50]. Upon phosphorylation and activation, AKT promotes Bad inactivation and its dissociation from mitochondria, increases the expression of the anti-apoptotic protein Bcl-2, and suppresses apoptotic signaling[51]. Therefore, based on the hypothesis that the CMW exerts protective effects against AMI through the SRC/PI3K/AKT signaling pathway, the expression levels of downstream apoptosis-related proteins Bcl-2 and Bax were further examined in this study. SRC/PI3K/AKT signaling and apoptosis regulation may contribute to the protective effects of CMW against AMI. These effects may be associated with the serum-absorbed constituents of CMW, including chlorogenic acid, neochlorogenic acid, naringin, afzelin, and quercitrin. Molecular docking analysis suggested that these compounds may interact with the core targets SRC, AKT, and PI3K.

During our exploration of how CMW regulates glycerophospholipid metabolism and the

PI3K/AKT pathway, a potential mechanistic connection between metabolic remodeling and signaling regulation was identified. Dysregulated glycerophospholipid metabolism may function as both a contributor to AMI progression and a consequence of impaired PI3K/AKT signaling, potentially creating a self-amplifying pathological loop that aggravates myocardial ischemic injury[52]. Such reciprocal dysregulation between metabolic processes and signaling cascades may contribute to sustained myocardial injury and impaired cardiac recovery during AMI progression[51]. CMW simultaneously ameliorated glycerophospholipid metabolic disturbances and activated the anti-apoptotic PI3K/AKT signaling pathway, which may represent a therapeutic advantage of its multi-component and multi-target properties compared with single-target interventions.

Conclusion

CMW ameliorated AMI-induced myocardial injury by restoring glycerophospholipid metabolic homeostasis and regulating the SRC/PI3K/AKT signaling pathway, with flavonoid and organic acid constituents, including chlorogenic acid, neochlorogenic acid, naringin, afzelin, and quercitrin, potentially representing key bioactive constituents contributing to its protective effects. This study provides new insights into the cardioprotective mechanisms of CMW by linking spatial glycerophospholipid metabolic remodeling with SRC/PI3K/AKT-mediated survival signaling, and highlights its potential value as a promising intervention for AMI management.

Abbreviations

AMI	acute myocardial infarction
BNP	B-type natriuretic peptide
CDDP	Compound Danshen Drop Pills
CK-MB	creatine kinase-MB
CMW	*Cinnamomum migao* water extract
cTnI	cardiac troponin I
GPC	glycerophosphocholine
LDH	lactate dehydrogenase
LPC	lysophosphatidylcholine
PA	phosphatidic acid
PC	phosphatidylcholine
PCho	phosphocholine

PS	phosphatidylserine
TTC	triphenyltetrazolium chloride

Author contributions

Z.Y.Z., Y.P., and L.Z. participated in the study design, material support, coordination, and supervision of the study. Z.Y.Z., Y.P., L.C., and C.X.Z. designed the experimental validation, performed experiments, analyzed the data, and drafted the manuscript. S.Y.C. and Y.T.L. carried out parts of the experiments. Z.P.G., M.Y.C., Y.H., and W.X.F. provided technical guidance. L.Z., Y.H., and W.X.F. provided constructive discussion regarding the experiments. All authors have read and approved the final manuscript. All data were generated in-house, and no paper mill was used. All authors agree to be accountable for all aspects of work ensuring integrity and accuracy.

Funding

This work was supported by National Natural Science Foundation of China (No. 82560837/82505182), Doctoral Program Foundation of Guizhou Medical University (J[2024]030/J[2025]042), Scientific and Technological Innovation Platform Research Project of Guizhou Province (CXPTXM [2025]010), Guizhou Science and Technology Department (Grant No. MS[2026]490/GCC [2022]031-2/ZD[2025]057/GCC[2023]036/QKHZC[2025]YB054), the Science and Technology Fund Project of the Guizhou Provincial Health Commission (Grant No. 2027GZWJKJXM1185), the Traditional Chinese Medicine and Ethnic Medicine Science and Technology Research Project of Guizhou Administration of Traditional Chinese Medicine (Grant No. QZYY-2027-077).

Data availability

No datasets were generated or analysed during the current study.

Declarations

Ethics approval and consent to participate

All animal procedures were conducted in accordance with institutional guidelines and approved by the Animal Ethics Committee of Guizhou Medical University (approval No. 2503507).

Competing interests

The authors declare no competing interests.

Author details

[1]State Key Laboratory of Discovery and Utilization of Functional Components in Traditional Chinese Medicine, School of Pharmaceutical Sciences, Guizhou Key Laboratory of Modern Traditional Chinese Medicine Creation, Guizhou Medical University, Anshun 561113, China. [2]National Engineering Research Center of Miao’s Medicines, Engineering Research Center for the Development and Application of Ethnic Medicine and TCM (Ministry of Education), Guizhou Medical University, Anshun 561113, China.

References

1. Zhu L, Liu Y, Wang K, et al. Regulated cell death in acute myocardial infarction: Molecular mechanisms and therapeutic implications. Ageing Res Rev. 2025, 104: 102629. http://dx.doi.org/10.1016/j.arr.2024.102629.
2. Yin M Q, Fan L H, Chen Y H. Typical clinical presentation of acute myocardial infarction and confusing coronary angiography: A case report and literature review of coronary embolism. Medicine (Baltimore). 2023, 102(19): e33782. http://dx.doi.org/10.1097/md.0000000000033782.
3. Lang Q, Qin C, Meng W. Appropriate Timing of Coronary Artery Bypass Graft Surgery for Acute Myocardial Infarction Patients: A Meta-Analysis. Front Cardiovasc Med. 2022, 9: 794925. http://dx.doi.org/10.3389/fcvm.2022.794925.
4. Xu Z, Meng F, Yang H, et al. BAK and BAX: Therapeutic Targets for Acute Myocardial Infarction and Myocardial Ischemia-Reperfusion Injury. Biology (Basel). 2025, 15(1): http://dx.doi.org/10.3390/biology15010081.
5. Paolisso P, Bergamaschi L, Saturi G, et al. Secondary Prevention Medical Therapy and Outcomes in Patients With Myocardial Infarction With Non-Obstructive Coronary Artery Disease. Front Pharmacol. 2019, 10: 1606. http://dx.doi.org/10.3389/fphar.2019.01606.
6. Shang P, Liu G G, Zheng X, et al. Association Between Medication Adherence and 1-Year Major Cardiovascular Adverse Events After Acute Myocardial Infarction in China. J Am Heart Assoc. 2019, 8(9): e011793. http://dx.doi.org/10.1161/jaha.118.011793.
7. Zullo A R, Mogul A, Corsi K, et al. Association Between Secondary Prevention Medication Use and Outcomes in Frail Older Adults After Acute Myocardial Infarction. Circ Cardiovasc Qual Outcomes. 2019, 12(4): e004942. http://dx.doi.org/10.1161/circoutcomes.118.004942.
8. Dai J, Qiu L, Lu Y, et al. Recent advances of traditional Chinese medicine against cardiovascular disease: overview and potential mechanisms. Front Endocrinol (Lausanne). 2024, 15: 1366285. http://dx.doi.org/10.3389/fendo.2024.1366285.
9. Fan J, Xia Z, Miao M, et al. Efficacy and safety of Shexiang Baoxin Pill combined with Baduanjin in the treatment of acute myocardial infarction: A prospective randomized study.

Medicine (Baltimore). 2025, 104(34): e44053. http://dx.doi.org/10.1097/md.0000000000044053.
10. Li C, Li Q, Xu J, et al. The Efficacy and Safety of Compound Danshen Dripping Pill Combined with Percutaneous Coronary Intervention for Coronary Heart Disease. Evid Based Complement Alternat Med. 2020, 2020: 5067137. http://dx.doi.org/10.1155/2020/5067137.
11. Tan L, Zeng C, Dong W, et al. Spatial Metabolomics Reveals GLA-Mediated Imbalance of Gal(2)Cer/GalCer as a Therapeutic Target in Myocardial Ischemia-Reperfusion Injury. Faseb j. 2026, 40(1): e71378. http://dx.doi.org/10.1096/fj.202502961RR.
12. White J B, Lin A, Montarello N J, et al. Changes to the serum lipidome and their relation to coronary plaque in the first six months after acute myocardial infarction. Atherosclerosis. 2025, 408: 120421. http://dx.doi.org/10.1016/j.atherosclerosis.2025.120421.
13. Guizhou Provincial Medical Products Administration. Quality Standards for Chinese Medicinal Materials and Ethnic Medicinal Materials of Guizhou Province (2019 Edition Volume 2). Beijing: China Medical Science Press, 2022.
14. Zeng X, Guo J, Xu J, et al. Integrating multi-omics and deep learning to explore the active ingredients and molecular mechanisms of *Cinnamomum migao* volatile oil in the treatment of coronary heart disease. Front Pharmacol. 2026, 17: 1823482. http://dx.doi.org/10.3389/fphar.2026.1823482.
15. Li X, Zhang Y, Dai W, et al. *Cinnamomum migao* Active Extracts Ameliorate Acute Myocardial Ischemia via Modulation of the HIF-1α/Nrf2/NF-κB/MAPK Pathway Downstream of Oxidative Stress. Antioxidants (Basel). 2026, 15(8): 970. http://dx.doi.org/10.3390/antiox15080970.
16. Sun X H, Sui Y H, Qiu D W. Protective effect of *Cinnamomum migao* on acute experimental myocardial ischemia in cats. Zhongguo Yaoxue Zazhi, 1995, 6: 341-344.
17. Gunata M, Parlakpinar H. A review of myocardial ischaemia/reperfusion injury: Pathophysiology, experimental models, biomarkers, genetics and pharmacological treatment. Cell Biochem Funct. 2021, 39(2): 190-217. http://dx.doi.org/10.1002/cbf.3587.
18. Pan W, Zhou G, Hu M, et al. Coenzyme Q10 mitigates macrophage mediated inflammation in heart following myocardial infarction via the NLRP3/IL1β pathway. BMC Cardiovasc Disord. 2024, 24(1): 76. http://dx.doi.org/10.1186/s12872-024-03729-x.
19. Wang J, Yu X, Wang T, et al. Metabolic changes of glycerophospholipids during the reparative phase after myocardial infarction injury. Front Cardiovasc Med. 2023, 10: 1122571. http://dx.doi.org/10.3389/fcvm.2023.1122571.
20. Tang H, Kan C, Zhang K, et al. Glycerophospholipid and Sphingosine- 1-phosphate Metabolism in Cardiovascular Disease: Mechanisms and Therapeutic Potential. J Cardiovasc Transl Res. 2025, 18(4): 749-761. http://dx.doi.org/10.1007/s12265-025-10620-3.
21. Jiang S, Lin X, Chen B, et al. ACSL1 Aggravates Thromboinflammation by LPC/LPA Metabolic Axis in Hyperlipidemia Associated Myocardial Ischemia-Reperfusion Injury. Adv Sci (Weinh). 2025, 12(11): e2406359. http://dx.doi.org/10.1002/advs.202406359.
22. Li X, Shi S, Yang Y, et al. The anticardiac fibrosis of total alkaloids of Plumula nelumbinis by regulating circulating lipidomic profile: In vivo study. J Food Biochem. 2022, 46(8): e14194. http://dx.doi.org/10.1111/jfbc.14194.
23. Xiao H, Sun X, Lin Z, et al. Gentiopicroside targets PAQR3 to activate the PI3K/AKT signaling pathway and ameliorate disordered glucose and lipid metabolism. Acta Pharm Sin B. 2022, 12(6): 2887-2904. http://dx.doi.org/10.1016/j.apsb.2021.12.023.
24. Han Q C. Study on Fuxin Decoction regulating the Nrf2/GPX4 signaling pathway to ameliorate

Doxorubicin-Induced ferroptosis in cardiomyocytes in heart failure; Shandong University of Traditional Chinese Medicine, 2025. http://dx.doi.org/10.27282/d.cnki.gsdzu.2025.000464.
25. Gao M, Jiang W, Cai Q, et al. Natural products and traditional Chinese medicine for myocardial infarction: A review of therapeutic mechanisms and applications. Chinese Herbal Medicines. 2026, http://dx.doi.org/https://doi.org/10.1016/j.chmed.2026.02.018.
26. Lv J, Pan C, Cai Y, et al. Plasma metabolomics reveals the shared and distinct metabolic disturbances associated with cardiovascular events in coronary artery disease. Nat Commun. 2024, 15(1): 5729. http://dx.doi.org/10.1038/s41467-024-50125-2.
27. Jiang C, Li D, Chen L, et al. Quercetin ameliorated cardiac injury via reducing inflammatory actions and the glycerophospholipid metabolism dysregulation in a diabetic cardiomyopathy mouse model. Food Funct. 2022, 13(14): 7847-7856. http://dx.doi.org/10.1039/d2fo00912a.
28. Bernardino de la Serna J, Vargas R, Picardi V, et al. Segregated ordered lipid phases and protein-promoted membrane cohesivity are required for pulmonary surfactant films to stabilize and protect the respiratory surface. Faraday Discuss. 2013, 161: 535-548; discussion 563-589. http://dx.doi.org/10.1039/c2fd20096a.
29. Rong J, He T, Zhang J, et al. Serum lipidomics reveals phosphatidylethanolamine and phosphatidylcholine disorders in patients with myocardial infarction and post-myocardial infarction-heart failure. Lipids Health Dis. 2023, 22(1): 66. http://dx.doi.org/10.1186/s12944-023-01832-0.
30. Law S H, Chan M L, Marathe G K, et al. An Updated Review of Lysophosphatidylcholine Metabolism in Human Diseases. Int J Mol Sci. 2019, 20(5): 1149 http://dx.doi.org/10.3390/ijms20051149.
31. Li L, Li L, Cao C, et al. Investigation of the active ingredients of Shuangshen Ningxin Fomula and the mechanism underlying their protective effects against myocardial ischemia-reperfusion injury by mass spectrometric imaging. Phytomedicine. 2024, 123: 155184. http://dx.doi.org/10.1016/j.phymed.2023.155184.
32. Wu J, Luo J, Cai H, et al. Expression characteristics of lipid metabolism-related genes and correlative immune infiltration landscape in acute myocardial infarction. Sci Rep. 2024, 14(1): 14095. http://dx.doi.org/10.1038/s41598-024-65022-3.
33. Tuboly E, Gáspár R, Ibor M O, et al. L-Alpha-glycerylphosphorylcholine can be cytoprotective or cytotoxic in neonatal rat cardiac myocytes: a double-edged sword phenomenon. Mol Cell Biochem. 2019, 460(1-2): 195-203. http://dx.doi.org/10.1007/s11010-019-03580-1.
34. Cao Q, Wang X, Jia L, et al. Inhibiting DNA Methylation by 5-Aza-2'-deoxycytidine ameliorates atherosclerosis through suppressing macrophage inflammation. Endocrinology. 2014, 155(12): 4925-4938. http://dx.doi.org/10.1210/en.2014-1595.
35. Schumacher D, Curaj A, Staudt M, et al. Phosphatidylserine Supplementation as a Novel Strategy for Reducing Myocardial Infarct Size and Preventing Adverse Left Ventricular Remodeling. Int J Mol Sci. 2021, 22(9): 4401. http://dx.doi.org/10.3390/ijms22094401.
36. Smeets S, Argenziano M E, De Crem A C, et al. Validation of the GPAT - the Global Polypectomy Assessment Tool: European Society of Gastrointestinal Endoscopy (ESGE) Position Statement. Endoscopy. 2025, 57(5): 555-566. http://dx.doi.org/10.1055/a-2541-4028.
37. Sarwar S, Randall G. HCV NS3/4A protease relocalizes CCTα to viral replication sites, enhancing phosphatidylcholine synthesis and viral replication. Proc Natl Acad Sci U S A. 2025, 122(10): e2419632122. http://dx.doi.org/10.1073/pnas.2419632122.

38. Soupene E, Fyrst H, Kuypers F A. Mammalian acyl-CoA:lysophosphatidylcholine acyltransferase enzymes. Proc Natl Acad Sci U S A. 2008, 105(1): 88-93. http://dx.doi.org/10.1073/pnas.0709737104.
39. Li H, Qiu Y, Xie M, et al. Momordicine I alleviates isoproterenol-induced cardiomyocyte hypertrophy through suppression of PLA2G6 and DGK-ζ. Korean J Physiol Pharmacol. 2023, 27(1): 75-84. http://dx.doi.org/10.4196/kjpp.2023.27.1.75.
40. Fukuchi M, Nakajima M, Fukai Y, et al. Increased expression of c-Ski as a co-repressor in transforming growth factor-beta signaling correlates with progression of esophageal squamous cell carcinoma. Int J Cancer. 2004, 108(6): 818-824. http://dx.doi.org/10.1002/ijc.11651.
41. Shang Q, Xu H, Huang L. Tanshinone IIA: A Promising Natural Cardioprotective Agent. Evid Based Complement Alternat Med. 2012, 2012: 716459. http://dx.doi.org/10.1155/2012/716459.
42. Ping P, Yang T, Ning C, et al. Chlorogenic acid attenuates cardiac hypertrophy via up-regulating Sphingosine-1-phosphate receptor1 to inhibit endoplasmic reticulum stress. ESC Heart Fail. 2024, 11(3): 1580-1593. http://dx.doi.org/10.1002/ehf2.14707.
43. Xiong G, Zou H, Hu C L, et al. Effects of chlorogenic acid on the proliferation and apoptosis of colon cancer cells mediated by P13k/Akt signaling pathway. Western Journal of Traditional Chinese Medicine, 2020, 33(5): 71-74
44. Yan Y W, Xiao L, Zhou X, et al. Pharmacological effects and pharmaceutical development strategies of chlorogenic acid. Zhongguo Yaofang, 2017, 28(19): 2729-2732.
45. Alam F, Kharya A K, Srivastav R K, et al. Synergetic Effect of Lupeol and Naringin Against Bile Duct Ligation Induced Cardiac Injury in Rats via Modulating Nitrite Level (eNos) and NF-kB /p65 Expression. Drug Res (Stuttg). 2023, 73(1): 23-29. http://dx.doi.org/10.1055/a-1879-2944.
46. Shackebaei D, Hesari M, Ramezani-Aliakbari S, et al. Cardioprotective effect of naringin against the ischemia/reperfusion injury of aged rats. Naunyn Schmiedebergs Arch Pharmacol. 2024, 397(2): 1209-1218. http://dx.doi.org/10.1007/s00210-023-02692-2.
47. Liu C Y, Fu Y, Li J W, et al. Quercitrin promotes M2 macrophage polarization after myocardial infarction in mice through the JAK2/STAT3 signaling pathway. Lingnan Modern Clinics in Surgery, 2025, 25(5): 302-311.
48. Chen K, Li G, Geng F, et al. Berberine reduces ischemia/reperfusion-induced myocardial apoptosis via activating AMPK and PI3K-Akt signaling in diabetic rats. Apoptosis. 2014, 19(6): 946-957. http://dx.doi.org/10.1007/s10495-014-0977-0.
49. Liu L, Liu X, Zhao L, et al. 1,8-cineole alleviates bisphenol A-induced apoptosis and necroptosis in bursa of Fabricius in chicken through regulating oxidative stress and PI3K/AKT pathway. Ecotoxicol Environ Saf. 2021, 226: 112877. http://dx.doi.org/10.1016/j.ecoenv.2021.112877.
50. Deng R M, Zhou J. The role of PI3K/AKT signaling pathway in myocardial ischemia-reperfusion injury. Int Immunopharmacol. 2023, 123: 110714. http://dx.doi.org/10.1016/j.intimp.2023.110714.
51. Chi Y, Ma Q, Ding X Q, et al. Research on protective mechanism of ibuprofen in myocardial ischemia-reperfusion injury in rats through the PI3K/Akt/mTOR signaling pathway. Eur Rev Med Pharmacol Sci. 2019, 23(10): 4465-4473. http://dx.doi.org/10.26355/eurrev_201905_17958.
52. Lei W, Yan Y, Ma Y, et al. Notoginsenoside R1 Regulates Ischemic Myocardial Lipid Metabolism by Activating the AKT/mTOR Signaling Pathway. Front Pharmacol. 2022, 13(905092. http://dx.doi.org/10.3389/fphar.2022.905092.

Supplementary Files

This is a list of supplementary files associated with this preprint. Click to download.

- SupplementaryMaterial.docx